EFDA–JET–PR(11)06

P. Maget, H. Lütjens, M. Brix, P. Buratti, R.J. Buttery, R. Coelho, F. Halpern,
N. Hawkes, I. Jenkins, C. Challis, C. Giroud, X. Litaudon, J. Mailloux,
N. Mellet, D. Meshcheriakov and JET EFDA contributors

Modelling of (2,1) NTM Dynamics with Flow in JET Advanced Scenarios

Modelling of (2,1) NTM Dynamics with Flow in JET Advanced Scenarios

P. Maget[1], H. Lütjens[2], M. Brix[3], P. Buratti[4], R.J. Buttery[5], R. Coelho[6], F. Halpern[2], N. Hawkes[3], I. Jenkins[3], C. Challis[3], C. Giroud[3], X. Litaudon[1], J. Mailloux[3], N. Mellet[1], D. Meshcheriakov[1] and JET EFDA contributors*

JET-EFDA, Culham Science Centre, OX14 3DB, Abingdon, UK

[1]CEA, IRFM, F-13108 Saint Paul-lez-Durance, France
[2]Centre de Physique Théorique, Ecole Polytechnique, CNRS, France
[3]EURATOM-CCFE Fusion Association, Culham Science Centre, OX14 3DB, Abingdon, OXON, UK
[4]ENEA, EURATOM Fusion Association, I-00040 Frascati, Italy
[5]General Atomics, PO Box 85608, San Diego, CA 92186-5608, USA
[6]Associação EURATOM/IST, Instituto de Plasmas e Fusão Nuclear, Instituto Superior Técnico, Av Rovisco Pais, 1049-001 Lisbon, Portugal
** See annex of F. Romanelli et al, "Overview of JET Results", (23rd IAEA Fusion Energy Conference, Daejon, Republic of Korea (2010)).*

Preprint of Paper to be submitted for publication in
Nuclear Fusion

ABSTRACT.
Experimental observations show that the β_N threshold for (2,1) NTM excitation is increased by flow shear, but the physical explanation for this trend is still unclear. In the present work, we investigate this issue by performing numerical experiments addressing the dependence of the critical island width on toroidal plasma rotation with the full MHD toroidal code XTOR [1], on the basis of a typical JET Advanced Tokamak case. We find that for situations where the Lundquist number is increased towards the experimental value, the (2,1) NTM is destabilized by flow shear at low magnetic Prandtl number Prm, while the threshold remains nearly insensitive to the flow at high Prm. The experimental trend is therefore not recovered, and possible explanations for this disagreement are discussed. A simple model of anisotropic viscous tensor shows that the high toroidal viscosity does not influence the value of the threshold, but comparison with experimental measurements suggests that the effective Prm seen by the mode is however larger than its small collisional value. Finally, the scaling of dimensionless parameters to ITER range is discussed.

1. INTRODUCTION

Large fusion devices like ITER will operate with little external momentum input, in contrast with most present tokamaks, and the sensitivity of the operational limits to plasma rotation has therefore received increasing interest in the last decade. Neoclassical Tearing Modes (NTM) are one of these limiting Magneto-Hydro-Dynamic (MHD) instabilities for which the extrapolation to ITER is a major issue, and a complex one too, due to their metastable nature. Indeed, NTMs are magnetic islands that are linearly stabilized by the combined effect of field line curvature and pressure gradient, but are non linearly destabilized by the bootstrap current perturbation [2]. The destabilization of these modes requires a primary mode, a coupling process with the island, and the seed that is thus produced must exceed a critical island width for entering the non linearly unstable NTM branch. These three ingredients (primary mode, coupling process, critical island) can all be affected by plasma rotation, although in different ways. In particular, there is no consensus on the response of the tearing mode to plasma flow and flow shear in realistic tokamak conditions. Early works in slab geometry with a reduced MHD model have shown that flow shear has first a destabilizing effect on the tearing mode in the sub- Alfvénic regime, either in inviscid [3, 4] or viscous plasma [5], before full stabilization is obtained for larger values of flow shear. However, reduced MHD models retaining perturbations parallel to the magnetic field ($\delta B_{||}$, $\delta V_{||}$) predict that flow shear becomes stabilizing when the plasma viscosity exceeds a threshold in cylindrical geometry [6], or even in inviscid plasma if toroidal geometry is accounted for, due to mode coupling [7]. In the non linear regime, predictions are also contrasted. Analytical work assuming a fully relaxed equilibrium in slab geometry predicts that the effect of flow and flow shear on the saturated tearing mode should be minor [8], while non linear simulations find that saturated islands are reduced in the presence of plasma rotation [9, 7]. In addition to this variety of results, it is not obvious that linear current-driven island physics and non linear pressure-driven NTM physics behave the same. The theoretical

basis for interpreting experiments on NTMs, where toroidal curvature stabilization [10, 11], heat transport properties [12], and bootstrap current are all potentially interacting with plasma flow, is therefore not firmly established.

Experiments have addressed an operational issue: establishing the plasma performance, expressed with β_N ($\beta_N = \beta aB/I_p^{MA}$, with $\beta = 2\mu_0 \langle p \rangle /B^2$, $\langle p \rangle$ is the volume average plasma pressure, a is the plasma minor radius, B is the magnetic field on axis, I_p^{MA} is the total plasma current expressed in MA), above which NTMs are triggered. The result of experimental analysis clearly shows that the critical N increases with plasma rotation [13, 14, 15], suggesting an increased (meta-)stability of the island. Moreover, the seeding process (primary mode and mode coupling) does not seem to be involved in this improved performance with rotation, suggesting that the dominant effect is on the intrinsic NTM stability in these discharges performed in the so-called "Hybrid scenario" with a safety factor $q(0) \sim 1$. This interpretation is supported by the observation of a reduction of saturated islands with increasing flow shear [16], suggesting a heuristic formula where the effective stability parameter Δ' decreases linearly when flow shear and magnetic shear length are increased. A coherent picture has been proposed after these experiments, which can be summarized as follow: at NTM triggering, the critical island width is close to zero due to the increase of Δ' as ideal limit is approached [17], and rotation shear allows approaching further the ideal limit by reducing Δ' [15]. Although experimental results could be explained with this model, its theory base and quantitative verification of its main feature (i.e. a stability improvement with rotation in linear as well as non linear regimes) is missing so far.

In the present work, we investigate numerically the impact of plasma flow on the critical island width for (2,1) NTM destabilization, i.e. on the intrinsic (meta)stability. Our tool is the non linear, full MHD, toroidal code XTOR [1], which has been used with a single fluid and a simplified bootstrap current model [18]. The reference equilibrium comes from a JET Advanced Tokamak discharge with $q > 1$, where a (2,1) NTM is observed. Its global stability properties may slightly differ from that of $q(0) \sim 1$ discharges that have been examined in the experimental studies of (2,1) NTM threshold with rotation mentioned above. However, the present work was initiated in the view of addressing this issue on the hypothesis that plasma flow could have a generic impact on tearing modes (we will come back on this hypothesis in the discussion). In contrast with previous works, we focus specifically on the NTM threshold issue, in conditions approaching the experimental ones, in terms of geometry, field description, and dimensionless plasma parameters, allowing a better understanding of what is behind the experimental trend.

The paper is organized as follows: physical model is described in section 2, experimental inputs in section 3, results on the effect of rotation on NTM threshold in section 4. Then we investigate the effect of a simple non isotropic viscous tensor (section 5), and the impact of resistivity in simulations (section 6). A discussion on the results obtained in the present work, and their link with experimental observations is developed in section 8, and a conclusion follows.

2. PHYSICAL MODEL

The effect of bulk plasma rotation on NTM is addressed in the framework of the standard single fluid MHD model:

$$\begin{aligned} \partial_t \rho + \nabla \cdot \rho \mathbf{V} &= r \cdot D_\perp \nabla \rho + \Sigma \\ \partial t p + \mathbf{V} \cdot \nabla p + \Gamma p \nabla \cdot V &= -(\Gamma - 1)\nabla \cdot \mathbf{q} + (\Gamma - 1)H \end{aligned} \quad (1)$$

$$\begin{aligned} \mathbf{q} &= -\rho \chi_\perp \nabla p/\rho - \rho\,(\chi_\parallel - \chi_\perp)\,\nabla_\parallel p/\rho \\ \partial_t \mathbf{B} &= \nabla \times (\mathbf{V} \times \mathbf{B}) - \nabla \times\ (\mathbf{J} - \mathbf{J_{NI}}) \end{aligned} \quad (2)$$

with $D_\perp$ the particle diffusion coefficient, $\Gamma = 5/3$, $\chi_\perp$ and $\chi_\parallel$ the perpendicular and parallel heat diffusivities. The density is restored by a particle source $\Sigma = -\nabla \cdot \chi_\perp \nabla p_{t=0}$, and the pressure is equilibrated by a heat source $H = -\nabla \cdot \chi_\perp \nabla p_{t=0}$. Here $\mathbf{J_{NI}} = \mathbf{J_{cd}} + \mathbf{J_{bs}}$ is the non inductive current density, $\mathbf{J_{bs}}$ is the bootstrap current, modelled as $\mathbf{J_{bs}} = J^{bs}_{eq}\,(\nabla p(t)/\nabla p^{eq})\mathbf{B}/B$, and $\mathbf{J_{cd}}$ is the imposed current source ($\mathbf{J_{cd}} = \mathbf{(J - J_{bs})}_{t=0}$).

We use a momentum equation of the form:

$$\rho\,(\partial_t \mathbf{V} + V \cdot \nabla\, \mathbf{B}) = J \times B - \nabla p + \nu \nabla^2\, \mathbf{V} + M \quad (3)$$

withthe viscosity, $M = -\nu \nabla^2\, \mathbf{V_{src}}$ the momentum source, and $\mathbf{V_{src}}$ the target toroidal velocity profile.

This system of equations is solved in toroidal geometry for up-down symmetric plasma cross-section, by the full MHD non linear code XTOR [1]. The magnetic equilibrium itself is computed with the CHEASE code [19], which also provides the equilibrium bootstrap current.

3. EXPERIMENTAL INPUTS

The experimental discharge that is considered corresponds to an Advanced Tokamak JET pulse performed at a magnetic field B = 1.8T, a plasma current $I_p = 1.2$MA, with a total additional beam power $P_{add} = 21$MW. The edge safety factor is $q_{95} = 5$, and a (2,1) NTM is triggered at t = 7.06s during the main heating phase, after an ELM crash. The NTM stability properties of this discharge have been described and studied for a static plasma in a previous work [20]. However, the central plasma rotation is at about 7% of the Alfvén speed, and the corresponding Mach number is M Section 1 36%, thus motivating a focus on this particular pulse for studying the impact of toroidal rotation.

In the following, we detail the input parameters that have been considered in the simulation: magnetic equilibrium, density and velocity profiles, diffusivity and viscosity. When moving from the real world to the virtual one that is offered by numerical simulations, our understanding of the physics phenomenon is greatly helped by the simplifications offered by the model, by the flexibility in the choice of parameters and by all possible synthetic diagnostics. However, computer limitations impose some restrictions on the accessible range of parameters, and non linear MHD simulations

are still limited in the choice of the plasma resistivity (η), which in the experimental range would lead to unreasonable spatial discretisation and computing time. The magnetic diffusivity $D\eta \equiv \eta/\mu_0$ is therefore chosen to be higher in the simulation compared to the experiment. The rescaling of resistivity that is applied imposes an appropriate rescaling of the other parameters, in order to keep the main physics similar to the real one. This results in

$$\tau_E/\tau_R \sim \mu_0 \chi_\perp/\eta = (\mu_0\chi_\perp/\eta)_{exp}.$$

allowing for a consistent dynamics of the plasma current (τ_R) with pressure driven bootstrap current (τ_E). However, in addition to the heat source H that depends on $\chi_\perp$, several physics parameters cannot be conserved in this transformation, like the size of the resistive layer ($\delta_{\eta,\nu}/\eta^{2/5}$), or the visco-resistive layer ($\delta_{\eta,\nu} \propto \eta)^{1/6}$ [21]), and the relative importance of convection ($\mathbf{V} \cdot \nabla p$) compared to diffusion ($\nabla \cdot \mathbf{q}$) in the pressure dynamics that governs the bootstrap drive. We will come back on this η-scaling issue in section 6, where the importance of investigating the trend towards the experimental Lundquist number will be demonstrated.

Other dimensionless parameters can be conserved as they are in experiments, like the magnetic Prandtl number Prm $\mu_0\nu/\eta$. This parameter is important in our study because of its role in the effect of flow shear on the linear tearing mode: at low Prm, flow shear has been found to be destabilizing, while the opposite holds at high Prm [6].

Another ratio that has a strong impact on the island dynamics is $\chi_\parallel/\chi_\perp$ [12]. It determines the characteristic island width above which perpendicular heat transport is no longer able to maintain the temperature gradient inside the separatrix. This ratio is particularly important in the context of NTMs, since it is related to the island size at which the bootstrap effect is maximum. It is therefore crucial to keep it constant in the rescaling procedure.

The analytical formulation of the neoclassical island dynamics can be written in the form of a so-called Generalized Rutherford Equation :

$$0.82S^{-1}\frac{dW}{dt} = a\Delta'(W) - 6.35\frac{D_R}{\sqrt{W^2 + 0.65W_\chi^2}} + 6.35\overline{J_{bs}}\frac{q}{s}\frac{W}{\sqrt{W^2 + (1.8W_\chi)^2}} \qquad (4)$$

where the various terms are evaluated at q = 2, S is the Lundquist number ($S = \tau_R/\tau_A$, with $\tau_R = \mu_0 a^2/\eta$ and $\tau_A = R_0\sqrt{\mu_0\rho/B_0}$), $\overline{J_{bs}}$ $(\mu_0 R_0/B_0)J_{eq}^{bs}$ with R_0 and B_0 the major radius and magnetic field at geometric axis, a the minor radius and $W \equiv w/a$. The characteristic length scale for the temperature flattening in the island is $W\chi = 2\sqrt{2}\,(\chi_\perp/\chi_\parallel)^{1/4}/x\epsilon ns$, with $x = \sqrt{\Phi}$, Φ is the normalized toroidal flux, $s = d(\log q)/d(\log x)$ the magnetic shear and $\epsilon = a/R_0$. The resistive index D_R, defined in [22], represents the stabilizing effect of field line curvature in a torus [10, 11]. In the Rutherford equation above, the Δ' parameter represents the drive for tearing instability coming from outside the resonant layer, and it is defined as

$$a\Delta'_0 = \lim_{\sigma\to 0}\frac{\psi'(x+\sigma) - \psi'(x+\sigma)}{\psi'(x_s)}$$

with ψ the perturbed poloidal magnetic flux, and x_s the radial position of the resonant surface. In the heuristic model of [15], an effect of flow on the effective Δ' was conjectured, in the form a $\Delta'(L_s, L_\omega) = a\Delta'_0 + CL_s/L_\omega$, with C a constant, $L_s = qR/s$ the magnetic shear length, and $a/L_\omega = a\, d(\omega/\omega A)/dR$ the rotation shear, with $\omega = V_\varphi/R$ and $\omega_A = VA/R0 = 1/\tau A$.

Despite allowing for a very useful and easy framework for understanding the physics of the NTM, the Rutherford equation has not an accurate predictive capability (in particular because of the absence of a reliable model for $\Delta'(W)$), as was shown for the saturated or critical island widths [23, 20]. Connexion between the flow and the pressure dynamics in our problem increases the complexity of the interactions between the separate pieces of the Rutherford equation (bootstrap, curvature, resistivity, and possibly Δ'). The use of comprehensive non linear MHD computations is therefore mandatory for clarifying the situation in real experiments, keeping in mind however that at least one dimensionless parameter, the Lundquist number S, cannot in general (as for the present work) be taken equal to its experimental value.

3.1. MAGNETIC EQUILIBRIUM

The magnetic equilibrium is taken from a reconstruction by EFIT code, constrained by Motional Stark Effect (MSE) measurements, as well as polarimetry and pressure measurements. Thus, the total pressure is an input from this equilibrium reconstruction. The separatrix is fitted in the mean least square sense by an up-down symmetric shape in order to be compatible with XTOR constraints, and the equilibrium is then computed again using the CHEASE code, which also provides the bootstrap current profile. The total bootstrap current fraction used in the simulations is $f_{bs} = 0.38$, a value that is close to the one given by the NCLASS module [24] implemented in TRANSP [25], which gives $f_{bs} = 0.34$. The local bootstrap current (at $q = 2$) represents 36% of the local parallel current.

3.2. DENSITY PROFILE

The density profile is given analytically in XTOR, but it fits very well the experimental one (as measured by LIDAR technique) up to the top of the pedestal region (figure 1).

3.3. VELOCITY PROFILE AND ITS SHEAR

Velocity shear, differential velocity (between the mode and its coupled harmonics), and absolute velocity could have different effects on the island dynamics. In toroidal geometry, differential velocity has been shown to be the most important stabilizing effect, while velocity shear at the resonance was reducing this stabilization [7]. In slab geometry, the effect of velocity shear is mixed with the absolute flow [4]. In order to address different situations, we have considered two different toroidal velocity sources having different velocities at $q = 2$ for the same rotation shear. These are expressed as functions of the normalized poloidal magnetic flux ψ as:

$$\text{Low V} : V_\varphi \propto (1 - \psi^2)^2\, p/\rho$$

$$\text{High V} : V_\varphi \propto (1 - 0.9\psi + 0.23\psi^4)$$

The two velocity profiles and the corresponding velocity shears are shown in figure 2, together with the experimental profile. Note that the implementation of the velocity source insures that with these sources the resulting equilibrium flow will have essentially a toroidal component and a negligible poloidal component.

We show in figure 3 the relation between the rotation shear and the plasma flow (normalized to the Alfvén velocity) at q = 2 (on the low magnetic side, at R = 3.55m). An error bar of 5cm in the position of q = 2 in the experiment has been considered for determining the error bars on the toroidal flow and the flow shear.

It is worth noting that the level of flow shear and magnetic shear length, in the experiment that is considered, is far below the point where full stabilization of the tearing mode was predicted in analytic theory [3, 4]. The stability condition in [4] is of the form $|G'| \geq |F'|$ with $F' = -a/L_s$, $G' = -\in/q(V + xa/L_\omega)$ and $\overline{V} = v/\overline{V}_A$, so that full stabilisation corresponds to:

$$\left|\frac{L_s}{L_\omega}\right| > \left|\frac{L_s}{L_\omega}\right|^{crit} \equiv \frac{q/\in}{x + VL_\omega/a}$$

In the experiment considered, we have (at q = 2 where $x \equiv \sqrt{\Phi} = 0.54$) $V \approx 0.03$, $a/L_\omega \approx -0.07$, $L_s/a \approx 7$, and $\in \equiv a/R_0 = 0.292$. This gives $|L_s/L_\omega| \approx 0.5$, while full stabilisation is predicted above the threshold value $|L_s/L_\omega|_{crit} \approx 60$. Note that the control parameter NFS $-L_s/L_\omega$ used to fit experimental results in [15], is in our case NFS ≈ 0.5. This is about the maximum value that has been obtained in these experiments, so that our study covers a comparable range of rotation shear as the experiments. For $|L_s/L_\omega| \approx 0.5$, the β_N threshold for (2,1) NTM was observed to be increased by one unit compared to the static case ($\beta_N \sim 3$ compared to $\beta_N \sim 2$). The rotation effect is therefore expected to be significant.

3.4. HEAT AND PARTICLE DIFFUSIVITES

The perpendicular heat diffusivity is determined in TRANSP from a power balance analysis (involving Neutral Beam and Ohmic heating in the experiment considered here). Since we evolve the total pressure, it is the effective diffusivity that is considered for XTOR simulations. The perpendicular diffusivities given by TRANSP and used in the simulations are shown in figure 4. The ratio $\chi_\parallel/\chi_\perp(0)$ is equal to 10^8 in the simulations, a value that is consistent with experimental evaluation taking into account the heat flux limit [20]. This gives $W_\chi = 0.038$ and a theoretical peak of the bootstrap drive at $W \approx 1.8W_\chi \approx 0.07$ following the analytical formulation of equation 4.

The particle diffusion coefficient $D_\perp$ is taken equal to $\chi_\perp$. The radial profile of $\chi_\perp$ and $D_\perp$ in XTOR are such that $\mu_0 \chi_\perp/\eta = C^{ste}$, an assumption that is reasonable for most of the plasma volume of interest for our study (the q = 2 surface is at $\sqrt{\Phi} = 0.54$) as shown in the bottom plot of figure 4. The parallel heat flux is taken as constant radially in the simulations.

3.5. VISCOSITY

Perpendicular plasma viscosity is generally expected to be small, allowing turbulence and MHD modes to develop as observed. From the theory of collisional transport in a magnetized plasma, the perpendicular viscous coefficient is [26, 27]:

$$v_{\perp coll} = 0.3 \frac{T_i \nu_i}{m_i \omega_{ci}^2}$$

with

$$\nu_i = \frac{4\sqrt{\pi}}{3} \frac{e^4 Z_i^4}{(4\pi\epsilon_0)^2} \frac{n_i \ln \Lambda}{m_i^{1/2} m_i^{3/2}}$$

the ion collision frequency, $\omega_{ci} = e_i B/m_i$ the ion cyclotron pulsation, and $\ln \Lambda \approx 17$. For the experimental case that is considered, we find $\mu_0 \nu_{\perp,coll.}/\eta \sim$ for $Z_i = 1$, but this value is underestimated due to the presence of impurity ions (the line integrated Z_{eff} is around 2.2). If we take for example $Z_i = Z_{eff}$, we get $\mu_0 \nu_{\perp,coll.}/\eta$ of the order of unity.

Anitropic viscous forces also arise from the neoclassical stress tensor. In the banana regime, the neoclassical viscous coefficient is proportional to the ion collision frequency: $\nu_{neo} \propto a^2 \nu_i$ [28], and is generally larger than the classical viscosity. We have not considered this component of the viscous tensor in the numerical applications, but we will come back on it in the discussion.

Finally, the viscous force in the toroidal direction can be determined experimentally from the toroidal momentum balance. This is done in the TRANSP code after calculating the torque induced by Neutral Beam Injection (NBI) into the plasma. The toroidal viscosity ν_φ is then found to be comparable to ion diffusivity, and about 2 orders of magnitude higher than the collisional estimate (figure 5). The connection between heat diffusivity and toroidal viscosity is explained by the fact that they are both consequences of the turbulent transport [29]. Note that, in the simulations, the viscosity coefficient is constant (in space and in time), leading to a non-constant radial profile of Prm. At q = 2 ($\sqrt{\Phi} \approx 0.54$), the actual value of Prm is about a factor 3 below its central value.

The extrapolation to ITER will depend on what part of the magnetic Prandtl number is important for the NTM dynamics. The toroidal part will give $Prm_\varphi \equiv \mu_0 \nu_\varphi/\eta \approx \mu_0 \chi_\perp/\eta \propto \beta/\nu^*$ if we assume a gyroBohm scaling of perpendicular diffusivity,with $\nu^* \equiv a/\nu_{Te}$ and $\nu_{Te} \sqrt{2T_e/m_e}$. The perpendicular part due to classical collisions will scale as $Prm_{coll.} \equiv \mu_0 \nu_\perp/\eta \propto \beta$ [26], while the neoclassical part will scale as $Prm_{neo} \equiv \mu_0 \nu_{neo}/\eta \propto \beta/\rho^{*2}$. Considering that the main changes will be on size (ρ^*) and collisionality in ITER, we can conclude that the perpendicular collisional Prm will not be significantly different in ITER, the neoclassical part will be a factor ~ 5 above the present JET case, while the toroidal part will be about one order of magnitude higher (using $a_{JET} \approx 0.86$m, $B_{JET} = 1.8$T, and $a_{ITER} \approx 2$m, $B_{ITER} \approx 5.3$T).

4. ROTATION EFFECT ON NTM THRESHOLD

4.1. PROCEDURE

The procedure for determining the critical island width is the following. First, the plasma rotation is

established with the prescribed source V_{src}. Since resistive modes are linearly stable, the non linear evolution only affects the n = 0 components at this stage. When a stationary n = 0 state is reached, a seed island is inserted into the plasma. This seed has been obtained by amplifying the bootstrap current by a large factor (a similar result can be obtained by reducing the Lundquist number to low values), allowing the tearing mode to enter a linearly unstable regime [30]. The size of the island is determined by a Poincaré plot of the field line trajectories, and converted in the normalized toroidal flux flux coordinate $\sqrt{\Phi}$ to give W = w/a. The seed island size is varied by a scaling factor, and increased stepwise until a non linear growth of the (2,1) mode energy is obtained.

For the simulations, we take $S(0) = 10^7$ (instead of $S(0) \sim 4 \times 10^8$ in the experiment). The radial resolution is 400 grid points, toroidal modes n = 0, 1 are evolved (we used 8 toroidal intervals to avoid aliasing), and the poloidal discretization consists of 128 Fourier modes.

As the island is inserted into the rotating plasma, oscillations of the magnetic energy are observed. Two examples of time evolution of the magnetic energy of the (2,1) mode are shown in figure 6, one at low Prm (left plot), and the other one at high Prm (right plot). Three characteristic pulsations are observed. At low viscosity (Prm = 2) and high rotation, oscillations at the Alfvén pulsation ($\omega_A = V_A/R_0$, $\omega_A(0) \equiv 1/\tau_A$ and $\omega_A\tau_A \approx 0.9$ at q = 2) are observed in the initial phase (as in figure 6, left plot). These Alfv´en waves have only been observed in a low Prm, high velocity case, and they are damped in about 100A. More commonly, energy oscillations at the sound wave pulsation ($\omega_s = c_s/R_0$ and $\omega_s \tau_A \approx 0.13$ at q = 2) are observed just after the introduction of the seed (as in the two examples of figure 6). They are damped in about $1000\tau_A$. Finally, oscillations slower than the sound wave frequency are observed (figure 6, right plot), and the pulsation of these oscillations depends on the equilibrium plasma flow shear rather than on the flow itself (figure 7). These waves need more than 10000A to be damped.

The comparison between experimental and simulation times requires a rescaling of the time scale

$$\Delta t_{[s]} = (D^{sim} / D^{exp}) \, \tau_A \Delta t$$

where $\bar{t}$ is the simulation time (normalized to the Alfvén time $\tau_A \approx 7.35 \times 10^{-7}$s) and $D_\eta \equiv \mu_0$ is the magnetic diffusivity. For simulations at $S = 10^7$, we have $D_\eta^{sim} / D_\eta^{exp} \approx 40$, and this translates into $\Delta t_{[s]} = 2.94 \times 10^{-5} \, \bar{t}$. Using this transformation rule, we can for example evaluate the characteristic time that is necessary for heat diffusivity to restore the pressure gradient in the seed: $\tau_\chi \sim w^2/\chi_\perp$. For the typical seed size W = w/a ~ 0.05 that we deal with in the present work, and with $\chi_\perp \sim 5m^2/s$ around q = 2 ($\sqrt{\Phi} = 0.54$), this gives a relatively short characteristic time τ_χ 4×10^{-4}s. In simulations performed at $S = 10^7$, this represents $(\tau_\chi/\tau_A)^{sim} = (D_\eta^{exp}/D_\eta^{sim})$ $(\tau_\chi/\tau_A)^{exp} \approx 10$. This value increases as the Lundquist number is increased towards its experimental value $S \sim 40\times10^7$, where $(\tau_\chi/\tau_A)^{exp} \approx 500$.

The neoclassical nature of the instability is revealed by looking at the bootstrap hole that develops at the O-point of the island. This is shown in figure 8 where a poloidal cross-section of the toroidal

component of the bootstrap current is plotted after the introduction of a seed Wseed = 0.053, together with a Poincar´e plot showing the island separatrix. In non linearly stable situations, this hole progressively vanishes, whereas it increases as the NTM branch is accessed. We quantify the hole in the bootstrap current by calculating $\delta J_{bs} \equiv J_{bs}^{X} - J_{bs}^{O}$, where X and O refer to the island X and O points.

4.2. NUMERICAL RESULTS

The value of the critical island width for the excitation of a (2,1) NTM has been determined for the two velocity profiles in the range of experimental flow shear, and for viscosities corresponding to Prm(0) equal 2 and 100. Detailed results for the 'High V' case with Prm=2 are shown in figure 9. From top to bottom, the figure shows the evolution of the island width on q = 2, the amplitude of the bootstrap perturbation Jbs, and the bootstrap at the O-point of the island. These plots are shown for the static case (left plot) and for rotating cases with increasing rotation shear (right plots). We only display here two levels corresponding to the highest stable (O) and the lowest unastable seed (▲). At an island size of about W Section 1 0.06, which corresponds approximatively to the critical size above which heat transport is no longer able to restore the pressure gradient (see section 3.4), the bootstrap at the O-point is close to zero (see bottom plot of the static case on the left). Then, the NTM enters a phase of negative bootstrap at the O-point. As saturation is approached and island growth slows down, the bootstrap at the O-point tends to zero. In simulations where momentum source is non-zero, the island and bootstrap dynamics are much softer, and become slower as rotation is increased. Equilibrium flow initially reduces the amplitude of the bootstrap current perturbation, before the non linear drive is (or not) taking over. In most cases with a non zero momentum source (except at Prm=100 and $S = 5 \times 10^7$, see section 6), the island dynamics is too slow to access the critical size where the bootstrap at the O-point becomes negative within the computation time necessary to discriminate between stable or unstable seed.

Results are shown in figure 10 as a function of the flow shear (left plot) and as a function of the flow (right plot) at q = 2.

The first observation is that for a given rotation profile, the variation of Prmbetween the collisional value and the turbulent one results in a significant increase of Wcrit, of about 20%. This motivates investigations on the behaviour of the MHD mode in a more realistic situation with anisotropic viscosity, for which a preliminary study is presented in the next section.

The second observation is that for a given Prm, the effect of plasma rotation on the critical island width is moderate (about 5% within the experimental range of a/Lω), Prm being small or large. This result is therefore not in agreement with experimental observations. Several possible explanations for this contradiction will be investigated in the following sections: a possible interplay between the direction of rotation and the anisotropic viscosity, or a role of the parameter domain in which simulations are performed, i.e. a role of the Lundquist number.

5. ANISOTROPIC VISCOUS TENSOR: RESULTS FROM A SIMPLE MODEL

We have seen that the magnetic Prandtl number has a significant impact on the NTM threshold, although this impact is weakly dependent on plasma rotation. In this section, we investigate the consequence of taking a non isotropic viscous tensor in the momentum equation. As a first step, we just separate the toroidal component of the viscous force, which we assume to be dominated by turbulent viscosity ($\nu_\varphi \approx \chi_\perp$ and Prm10 100), from the other components which we assume to be dominated by collisional viscosity $\nu \approx \nu_{coll}$ and Prm ~ 2). The momentum equation is then:

$$\rho\,(\delta_t \mathbf{V} + \mathbf{V}\cdot\nabla\mathbf{V}) = \mathbf{J}\times\mathbf{B} - \nabla p + \nu\nabla^2\mathbf{V} + (\nu_\varphi - \nu)(\nabla^2\mathbf{V})_\varphi + \mathbf{M} \qquad (5)$$

with a momentum source $\mathbf{M} = -(\nu_\varphi - \nu)\nabla^2\mathbf{V}_{\mathbf{src}}$. In the toroidal direction, we get therefore to leading order a viscous force $F_\varphi \approx \nu_\varphi\, d^2(V')/dx^2$ that is formally comparable to the toroidal momentum diffusion driven by turbulence.

The critical island width for anisotropic viscosity is found to be dominated by the collisional, non toroidal, component of the viscous force (see figure 11). This result is consistent with the usual picture that MHD perturbations develop in the direction perpendicular to the magnetic field, but the results obtained in reduced MHD with parallel components seemed to suggest that they could play a role in presence of rotation. Our simulations show that it is not the case (at least with the simple anisotropic model we used). The only signature of the higher toroidal viscosity is the stronger damping of Alfvén waves, as shown in the right plot of figure 11.

We can therefore conclude that the dimensionless parameter Prm that is used in simulations should not be based upon its toroidal component, but rather upon its perpendicular component. The classical value that we have considered here scales like and is therefore in the correct range for extrapolating to ITER. However, the neoclassical part, which we have not considered here but scales as β/ρ^2, will be higher in ITER.

6. INVESTIGATIONS AT HIGHER LUNDQUIST NUMBER

In this section, we investigate the validity of the -scaling rule, by computing the critical island width at a smaller magnetic diffusivity D_η (closer to the experimental one) while keeping other dimensionless parameters (Prm, $\mu_0\chi_\perp/\eta$ and $\chi_\parallel/\chi_\perp$) constant. In the experiment, the Lundquist number at magnetic axis is about $S \approx 40\times10^7$, i.e. a factor ~40 above the one used in previous simulations. We have thus performed numerical experiments at $S = 2\times10^7$ in order to assess the impact of this parameter on the non linear NTM threshold.

As mentioned earlier, the rescaling imposed by taking a larger resistivity in the simulation has consequences on the width of the resistive layer, ($\delta_\eta \propto S^{-2/5}$), or the visco-resistive layer ($\delta_{\eta,\nu} \propto \mathrm{Prm}^{1/6} S^{-1/3}$ [21]), on the heat source H, and on the relative importance of convection and diffusion in the pressure dynamics that governs the bootstrap drive. Indeed, with $\mu_0\chi_\perp/\eta = C^{ste}$, the convection term $\mathbf{V}\cdot\nabla p$ is unchanged as S is increased in the simulations, diffusion term will be smaller since $\chi_\perp\nabla_\perp^2 p = C^{ste}S^{-1}\nabla_\perp^2 p$ and $\chi_\parallel^2 p = C^{ste}S^{-1}(\chi_\parallel/\chi_\perp)\nabla_\parallel^2 p$.

We use the equivalent real time scale (see section 4) for comparing simulations at different Lundquist numbers.

We show in figure 12 the island dynamics just below and above the threshold at $S = 10^7$ and $S = 2 \times 10^7$, in the low Prm regime (Prm=2). The island evolution is slower, and it takes more time to discriminate between stable and unstable seeds. But considering the first $20\times10^3\tau_A$ ($\Delta t_{[s]} \sim 0.3s$), it appears that the lowest unstable seeds at $S = 10^7$ (circles) are stable at $S = 2 \times 10^7$ for finite flow cases. The threshold is therefore moving up when increasing S, and the change is more significant for finite but small flow, resulting in a destabilizing effect of flow.

For the static case (no rotation source), the opposite trend seems to hold, with a slightly lower threshold at $S = 2 \times 10^7$. The apparent saturation at $S = 2 \times 10^7$ for the static case is significantly below its size at $S = 10^7$. This may correspond either to a state that is not the final saturation of the island, or indicate a dependence of saturated width on the Lundquist number (note that a reduction of saturation width while increasing S was also reported in [31] using a cylindrical reduced MHD non linear model).

At high Prm, numerical constraints are less stringent due to the damping of small structures, allowing in addition larger time steps. Investigations could therefore be extended to $S = 5\times10^7$. The island dynamics above and below the threshold are shown in figure 13. Several observations can be made. First, the conversion into the equivalent experimental time shows that the NTM dynamics predicted by the simulation becomes faster as S is increased. Second, the perturbed bootstrap current δJ_{bs} that remains after the initial transitory phase is increasing with S, although the seed is comparable or smaller. This points towards a role of the heat source in this change: at lower S, the heat source is larger due to the $S\chi_\perp$ scaling rule, and may partly compensate for the bootstrap hole created by the seed. Although the consequence on the critical island width is not important up to $S = 2 \times 10^7$, this phenomenon results in a significant decrease of W_{crit} in the $S = 5 \times 10^7$ simulations. This effect is however absent in low Prm simulations, where after the transitory phase δJ_{bs} is lower at higher S for the same seed (see symbols in figure 12).

These numerical experiments accross the Lundquist parameter domain show the complexity of the NTM behaviour in presence of flow, where different physics mechanisms are at play for deciding on the non linear behaviour of the mode. We find that both the critical island width and the effect of rotation are strongly affected when moving closer to the experimental domain in S while keeping other dimensionless parameters constant, and the value of the magnetic Prandtl number is playing a crucial role in determining the overall trend. The picture that emerges can be summarized as follows (figure 14).

- At low Prm, the static case behaves differently compared to the rotating ones, with a thresholds that decreases with S. But from the lowest rotating case considered, increasing S stabilises the NTM, resulting in a higher non linear threshold. However, this stabilization is less effective as rotation shear is higher. As a result, closer to the experimental domain in S, a clear destabilizing effect of rotation shear appears.

- At high Prm, moving to higher S leads to a more unstable NTM (lower non linear threshold), an effect that could be due to the lower heat source, and would be therefore a consequence of the -scaling rule which links S and ?. Rotation shear does not affect significantly the value of the non linear threshold, in the range of S that is covered.

These results are reminiscent of some properties previously obtained in the linear regime. For example, they suggest both a change of the rotation effect with Prm, and a S-dependence of this change, as found in [6]. However, no stabilizing effect of rotation is found in the high Prm regime up to $S = 5 \times 10^7$. This may appear above the S range that has been addressed. Also, the dynamics of the mode reacts differently to the change of the Lundquist number at low and high Prm. In presence of rotation, the mode dynamics in the viscous regime (Prm = 100) is faster when increasing S. This is reminiscent of the linear regime with viscosity, where indeed the growth rate could be comparable or higher in presence of finite viscosity in situations of significant rotation shear (whereas high viscosity otherwise reduces the growth rate) [5]. Besides these links with the linear tearing mode behaviour, our simulations show that the overall NTM stability in rotating plasma is determined by competing mechanisms and results in a more complex picture.

7. NTM AND ITS IMPACT ON EQUILIBRIUM FLOW

In this section we investigate the effect of the magnetic island on the plasma flow. The radial structure of the n = 0 component of the toroidal flow and toroidal flow shear along the equatorial plane in the experiment and for the "High V" case that is the closest to the experiment, with Prm = 100 and Prm = 2, are shown in figure 15. We note $t_0 = 7.06$s the time when the (2,1) NTM is triggered in the experiment, and the equivalent experimental time is computed as explained earlier: $\Delta t_{[s]} = 2.94 \times 10^{-5}\, \bar{t}$ (for $S = 10^7$).

We find that the presence of the NTM does not strongly affect the toroidal rotation in the Prm = 100 simulation. Conversely, at Prm = 2, the equilibrium toroidal flow has a fine dipolar structure around the resonance that is generated by the island. This equilibrium flow generation also exists in simulations with anisotropic viscosity, and is therefore associated with the low perpendicular Prm. In the experiment, no significant modification of the toroidal rotation profile is seen by the Charge Exchange diagnostic during the island growth. In order to do better comparison between experiment and simulation, we calculate the toroidal rotation profile at a radial resolution corresponding to that of the Charge Exchange diagnostic ($\Delta R \sim 7$cm, while the radial resolution of the simulation is ($\Delta R \sim 0.2$cm). We resample the equilibrium toroidal velocity profile from XTOR using all possible combination of points equally spaced by 7cm, thus getting a set of 35 synthetic diagnotics having the specified radial resolution but different lines of sight. We then compute the average radial position, the average toroidal velocity and the average velocity shear parameter a/L_ω from the set of synthetic Charge Exchange diagnostic. The error bar corresponds to the difference between the extremum and the averaged values. This excercice shows that the fine dipole structure produced

by the (2,1) NTM is not easily accessible from the Charge Exchange diagnostic in general, except when the lines of sight are close enough to the island position where the modification of the equilibrium flow could be observed. The absence of this structure in the measurement does not formally prove that Prm is larger than 2, but it suggests at least that a larger Prm is more likely to be applicable to this plasma.

8. DISCUSSION

The main results that have been obtained and reported in this paper are the following:

- Investigations in the Lundquist number domain while keeping other dimensionless parameters constant has proved to be essential for extrapolating to experimental regimes. Indeed, exploring various S has evidenced significant variations of the non linear threshold as well as its dependence on rotation shear.
- Extrapolating the trend that is found towards realistic values of the Lundquist number suggests that rotation shear has a destabilizing effect at low Prm and a neutral effect at high Prm. This is similar to the picture obtained previously in the linear regime, except that the stabilizing effect is not recovered. In terms of absolute NTM threshold, we find opposite trends at high and low Prm, with a more stable NTM at low Prm compared to high Prm.
- A large toroidal component of Prm does not affect significantly the behaviour of the island which remains influenced by the perpendicular Prm.

The reason why experimental observations, showing such a stabilizing influence of rotation, are not recovered in simulations, could originate from different factors:

- Non linear simulations are not performed with the adequate physics model: by investigating NTM frequency in the plasma frame, experimental observations did not evidence any role of polarization effect [13], so that using a bi-fluid model is not expected to better reproduce the physical mechanism at work in experiments from this effect. However, the viscous tensor model is still very simple, and a more realistic description of viscous forces would be desirable. In particular, the poloidal rotation associated to the neoclassical presure tensor could affect the threshold more than the toroidal rotation that has been investigated here, although the rotation dependence of the NTM threshold that has been reported experimentally relates to scans of the toroidal rotation.
- Non linear simulations are not in the proper parameter domain: as indicated by our η-scaling, it may be that going to relevant Lundquist numbers, with a relatively large Prm due to neoclassical physics, the NTM threshold would become much smaller and possibly lead to seedless triggering, i.e. linearly unstable island. The effect of rotation does not seems to become more clearly stabilizing at high S, but we still remain a factor ~8 below the experimental value however.
- Non linear simulations are not addressing the same kind of equilibrium as the original experiments. In particular, we are far enough from ideal limit to get relatively large threshold

for NTM excitation, in contrast with the experiments for which the threshold is suspected to be very small due to the so-called "Δ' pole". The boundary condition of our numerical simulations (ideal wall at the plasma boundary), tends to push the ideal limit to higher values that in the experiment, and may result in missing the 0 increase. In addition, a role of the ideal instability in the NTM triggering itself is not to be excluded, as a ballooned kink-like structure is often observed in the initial phase of the NTM growth as reported in [32, 20]. As mentionned above, however, if Prm is large, small NTM threshold can also be expected at large S.

Another output from our work concerns the role of plasma viscosity (through the magnetic Prandtl number Prm) in the dynamics of NTMs. We find that the toroidal Prm, that is deduced from toroidal momentum balance and explained by the connection between the anomalous heat diffusivity and its momentum counterpart, does not impact significantly the dynamics of the NTM, which remains dominated by the perpendicular viscosity. However, we have indications that the Prm value deduced from classical collisions is too weak to reproduce the observed non linear dynamics of the mode. First, the time scale of the NTM growth in the experiment was found to be similar to the static case [20]. This means that the low Prm case results in a dynamics that is too slow compared to the experimental one. It is only in the high Prm simulations that we have a growth that is not damped by plasma flow. Second, the impact of the mode on the equilibrium toroidal flow does not show any sign of the dipole structure expected from simulations at Prm = 2. Although the resolution of the diagnostic does not allow excluding a situation where the line of sight would miss this structure, it seems more likely that this structure is simply absent, as in simulations with Prm = 100. The fact that the perpendicular Prm could be influenced by neoclassical physics in present and future plasma experiments suggests that Prm could be significantly larger than its collisional value, and will be even larger in ITER because it scales as β/ρ^{*2}. Note however that the dimensionless parameter Pr/Prm $\mu_0\chi_\perp/\eta_\perp$ will also be higher since it scales as The role of this parameter in the NTM threshold and its sensitivity to plasma rotation remains to be addressed in more details, but previous simulations performed at $S = 10^7$ indicated lower (2,1) NTM thresholds at both low and high Prm when $\mu_0\chi_\perp/\eta$ was increased from 150 to 600 [33].

CONCLUSIONS

In the present work, the dependence of (2,1) NTM threshold on rotation has been addressed by performing numerical experiments with a full MHD non linear code in toroidal geometry. These investigations, based on a representative Advanced Tokamak discharge from JET, were intended to better understand experimental results showing an increase of the N threshold for (2,1) NTM triggering as rotation shear (and more precisely L_s/L_ω) was increased. We find that plasma rotation tends to have a destabilizing effect on NTMs at low Prm, while it remains neutral at high Prm in the range of Lundquist number that has been investigated. The use of a simple anisotropic viscous

tensor also demonstrates that it is the perpendicular (to the magnetic field) value of Prm that matters for the NTM dynamics. The favourable effect of rotation that is found experimentally is therefore not a generic feature. We envisage two main possibilities for the disagreement between our numerical investigations and experimental observations. First, the domain of resistivity that has been investigated could be still too far from the experiment, since we find that the resistivity scaling influences both the NTM threshold and the effect of rotation. The second possibility is that we address a situation with relatively large thresholds while experimental observations report seedless or marginal thresholds due to the proximity to ideal limit. The favourable influence of rotation may therefore be enhanced in situations where the island is closer to marginal stability, or where an ideal mode (modified by finite plasma or wall resistivity), similar to the kink-like structure that is sometimes observed on JET, is contributing to the NTM growth. Finally, investigating the viscosity issue in a more comprehensive neoclassical model would be desirable, with an associated Prm that scales like β/ρ^{*2}, and will become higher in ITER.

ACKNOWLEDGMENTS

This work was carried out within the framework of the European Fusion Development Agreement (EFDA) and the French Research Federation for Fusion Studies (FR-FCM). It was performed using HPC resources from GENCI-IDRIS (Grants 2010-056348 and 2011-056348) and CCRT (Centre de calcul Recherche et Technologie of CEA). It is supported by the European Communities under the contract of Association between Euratom and CEA. The views and opinions expressed herein do not necessarily reflect those of the European Commission.

REFERENCES

[1]. Hinrich Lütjens and Jean-François Luciani. XTOR-2F: A fully implicit Newton-Krylov solver applied to nonlinear 3D extended MHD in tokamaks. Journal of Computational Physics, **229**(21):8130 – 8143, 2010.

[2]. R. Carrera, R. D. Hazeltine, and M. Kotschenreuther. Island bootstrap current modification of the nonlinear dynamics of the tearing mode. Physics of Fluids, **29**(4):899–902, 1986.

[3]. G. Einaudi and F. Rubini. Resistive instabilities in a flowing plasma: I. inviscid case. Physics of Fluids, **29**(8):2563–2568, 1986.

[4]. X. L. Chen and P. J. Morrison. Resistive tearing instability with equilibrium shear flow. Physics of Fluids B, **2**(3):495, 1990.

[5]. Giorgio Einaudi and Franco Rubini. Resistive instabilities in a flowing plasma. II. effects of viscosity. Physics of Fluids B: Plasma Physics, **1**(11):2224–2228, 1989.

[6]. R. Coelho and E. Lazzaro. Effect of sheared equilibrium plasma rotation on the classical tearing mode in a cylindrical geometry. Physics of Plasmas, **14**(1):012101, 2007.

[7]. D. Chandra, A. Sen, P. Kaw, M.P. Bora, and S. Kruger. Effect of sheared flows on classical and neoclassical tearing modes. Nuclear Fusion, **45**(6):524, 2005.

[8]. F.L. Waelbroeck, R. Fitzpatrick, and Daniela Grasso. Effect of sheared flow on magnetic islands. Physics of Plasmas, **14**(2):022302, 2007.

[9]. L. Ofman, P.J. Morrison, and R. S. Steinolfson. Nonlinear evolution of resistive tearing mode instability with shear flow and viscosity. Physics of Fluids B: Plasma Physics, **5**(2):376–387, 1993.

[10]. M. Kotschenreuther, R. D. Hazeltine, and P. J. Morrison. Nonlinear dynamics of magnetic islands with curvature and pressure. Physics of Fluids, **28**(1):294–302, 1985.

[11]. Hinrich Lütjens, Jean-Fran¸cois Luciani, and Xavier Garbet. Curvature effects on the dynamics of tearing modes in tokamaks. Physics of Plasmas, 8(10):4267–4270, 2001.

[12]. Richard Fitzpatrick. Helical temperature perturbations associated with tearing modes in tokamak plasmas. Physics of Plasmas, **2**(3):825–838, 1995.

[13]. R.J. Buttery, R.J. La Haye, P. Gohil, G.L. Jackson, H. Reimerdes, E.J. Strait, and the DIIID Team. The influence of rotation on the betan threshold for the 2/1 neoclassical tearing mode in DIII-D. Physics of Plasmas, 15(5):056115, 2008.

[14]. S.P. Gerhardt, D.P. Brennan, R. Buttery, R.J. La Haye, S. Sabbagh, E. Strait, M. Bell, R. Bell, E. Fredrickson, D. Gates, B. LeBlanc, J. Menard, D. Stutman, K. Tritz, and H. Yuh. Relationship between onset thresholds, trigger types and rotation shear for the m / n = 2/1 neoclassical tearing mode in a high-beta spherical torus. Nuclear Fusion, 49(3):032003, 2009.

[15]. R.J. La Haye, D. P. Brennan, R. J. Buttery, and S. P. Gerhardt. Islands in the stream: The effect of plasma flow on tearing stability. Physics of Plasmas, 17(5):056110, 2010.

[16]. R. J. La Haye and R. J. Buttery. The stabilizing effect of flow shear on m/n = 3/2 magnetic island width in DIII-D. Physics of Plasmas, 16(2):022107, 2009.

[17]. D.P. Brennan, R.J. La Haye, A.D. Turnbull, M.S. Chu, T.H. Jensen, L.L. Lao, T. C. Luce, P.A. Politzer, E.J. Strait, S. E. Kruger, and D. D. Schnack. A mechanism for tearing onset near ideal stability boundaries. Physics of Plasmas, **10**(5):1643–1652, 2003.

[18]. H. Lütjens. Toroidal simulations of nonlinear thresholds and saturations of classical and neoclassical tearing instabilities. Computer Physics Communications, **164**(1-3):286 – 290, 2004. Proceedings of the 18th International Conference on the Numerical Simulation of Plasmas.

[19]. H. Lütjens, A. Bondeson, and O. Sauter. The CHEASE code for toroidal MHD equilibria. Computer Physics Communications, **97**(3):219–260, 1996.

[20]. P. Maget, H. Lütjens, R. Coelho, B. Alper, M. Brix, P. Buratti, R.J. Buttery, E. De la Luna, N. Hawkes, G.T.A. Huysmans, I. Jenkins, C.D. Challis, C. Giroud, X. Litaudon, J. Mailloux, M. Ottaviani, and JET-EFDA Contributors. Modelling of (2,1) NTMthreshold in JET advanced scenarios. Nuclear Fusion, **50**(4):045004, 2010.

[21]. Francesco Porcelli. Viscous resistive magnetic reconnection. Physics of Fluids, **30**(6):1734–1742, 1987.

[22]. A.H. Glasser, J. M. Greene, and J. L. Johnson. Resistive instabilities in general toroidal plasma configurations. Physics of Fluids, **18**(7):875–888, 1975.

[23] Hinrich Lütjens and Jean-Fran¸cois Luciani. Saturation levels of neoclassical tearing modes in International Thermonuclear Experimental Reactor plasmas. Physics of Plasmas, **12**(8):080703, 2005.

[24]. W. A. Houlberg, K. C. Shaing, S. P. Hirshman, and M. C. Zarnstorff. Bootstrap current and neoclassical transport in tokamaks of arbitrary collisionality and aspect ratio. Physics of Plasmas, **4**(9):3230–3242, 1997.

[25]. R.J Goldston, D.C McCunea, H.H Towner, S.L Davis, R.J Hawryluk, and G.L Schmidt. New techniques for calculating heat and particle source rates due to neutral beam injection in axisymmetric tokamaks. Journal Computational Physics, **43**:61, 1981.

[26]. S.I. Braginskii. Transport processes in plasma. In M.A. Leontovich, editor, Review of Plasma Physics, volume 1 of Review of Plasma Physics, pages 201–311. Consultants Bureau, New York, U.S.A., 1965.

[27]. D. Biskamp. Drift-tearing modes in a tokamak plasma. Nuclear Fusion, 18:1059, 1978.

[28]. S. P. Hirshman and D. J. Sigmar. Neoclassical transport of impurities in tokamak plasmas. Nuclear Fusion, **21**(9), 1981.

[29]. A. G. Peeters, C. Angioni, and D. Strintzi. Toroidal momentum pinch velocity due to the coriolis drift effect on small scale instabilities in a toroidal plasma. Physical Review Letters, **98**(26):265003, Jun 2007.

[30]. Hinrich Lütjens and Jean-François Luciani. Linear and nonlinear thresholds of neoclassical tearing modes in tokamaks. Physics of Plasmas, **9**(12):4837–4840, 2002.

[31]. Q. Yu, S. Gunter, and K. Lackner. Numerical modeling of nonlinear growth and saturation of neoclassical tearing modes. Physics of Plasmas, **11**(1):140–150, 2004.

[32]. P. Buratti, C.D. Challis, M. Gryaznevich, T.C. Hender, E.Joffrin, T. Luce, P. Smeulders, and JETEFDA contributors. Radial analysis of beta-limiting modes in JET. 35th EPS Conf. on Plasma Physics, Hersonisos (Greece), (P1.069), European Physical Society, 2008.

[33]. P. Maget, H. Lütjens, B. Alper, M. Baruzzo, M. Brix, P. Buratti, R. Buttery, C. Challis, R. Coelho, E. De la Luna, C. Giroud, N. Hawkes, G. Huysmans, I. Jenkins, X. Litaudon, J. Mailloux, N. Mellet, D. Meshcheriakov, M. Ottaviani, and JET EFDA contributors. Effect of rotation on the modelled NTM threshold in JET advanced scenarios. 37th European Physical Society Conference On Plasma Physics, Dublin (Irland), (O2.104), European Physical Society, 2010.

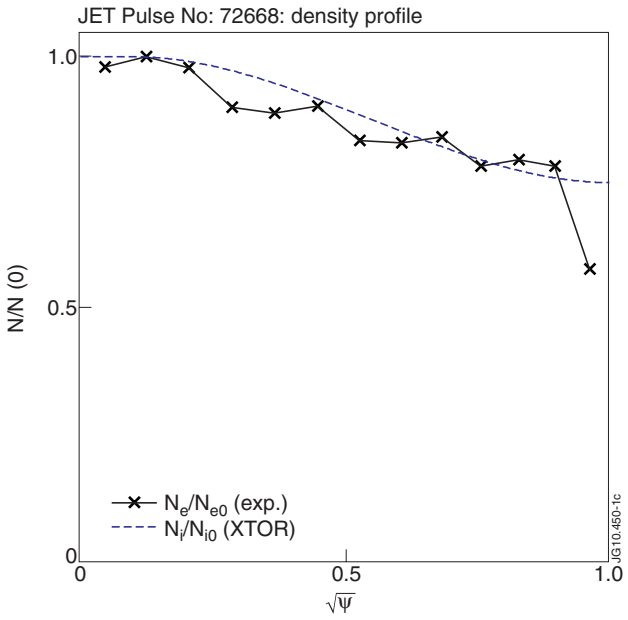

Figure 1: Density profile: experiment and simulation inputs.

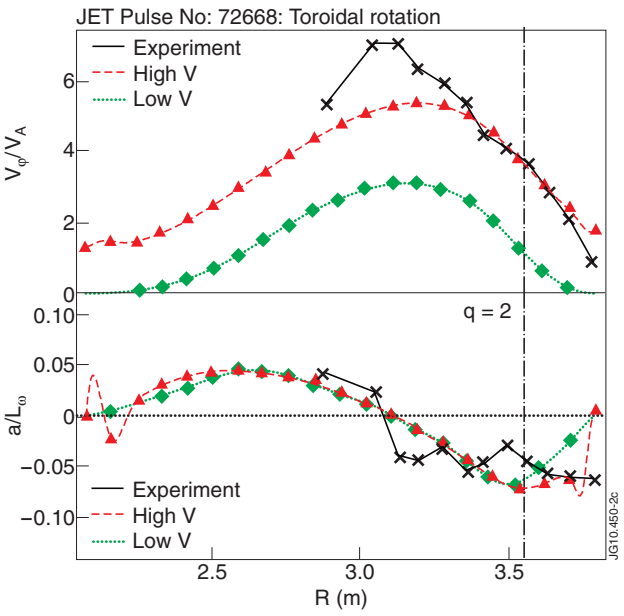

Figure 2: Toroidal rotation (top) and rotation shear (bottom) profiles: experiment and simulation inputs. The position of q = 2 in the simulations is indicated.

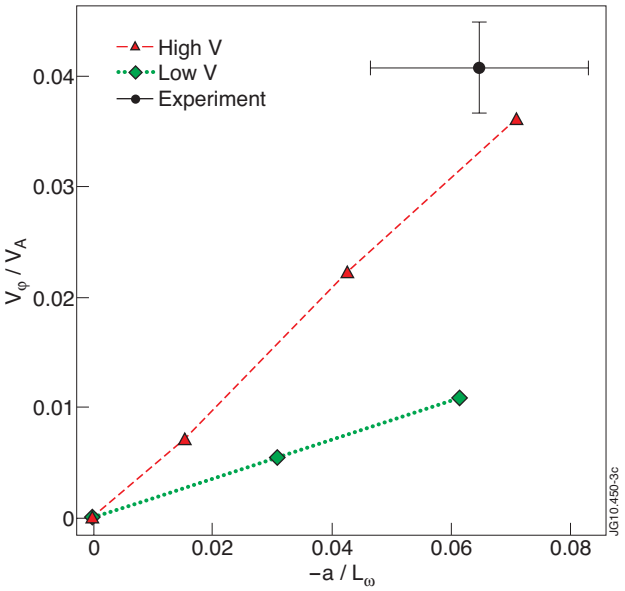

Figure 3: Rotation versus rotation shear: experiment and simulation inputs.

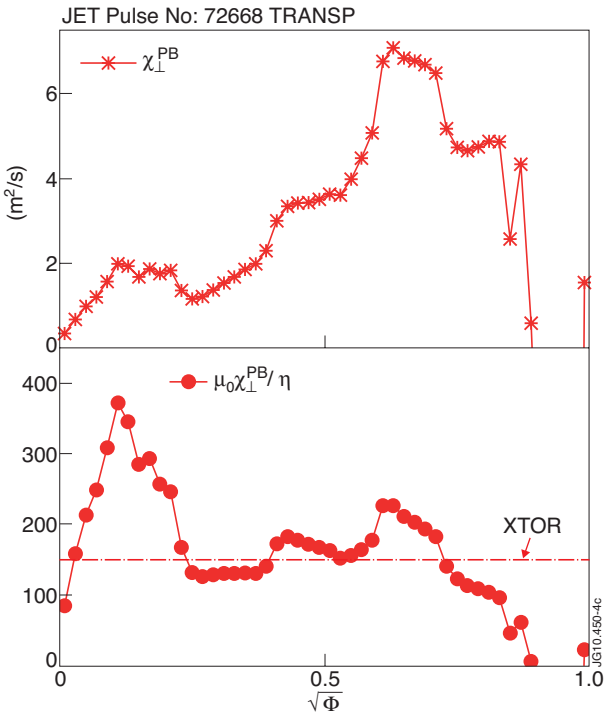

Figure 4: Heat diffusivity (top) and ratio Prm/Pr (bottom) from TRANSP. The values used in XTOR simulations are shown with dashed lines in the bottom figure.

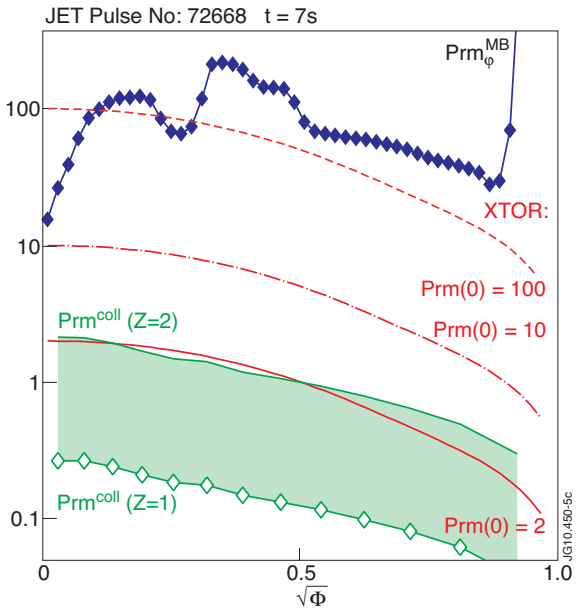

Figure 5. Collisional Prandtl number for $Z_i = 1$ and $Z_i = 2$, and toroidal Prandtl number from Momentum Balance (MB) in TRANSP.

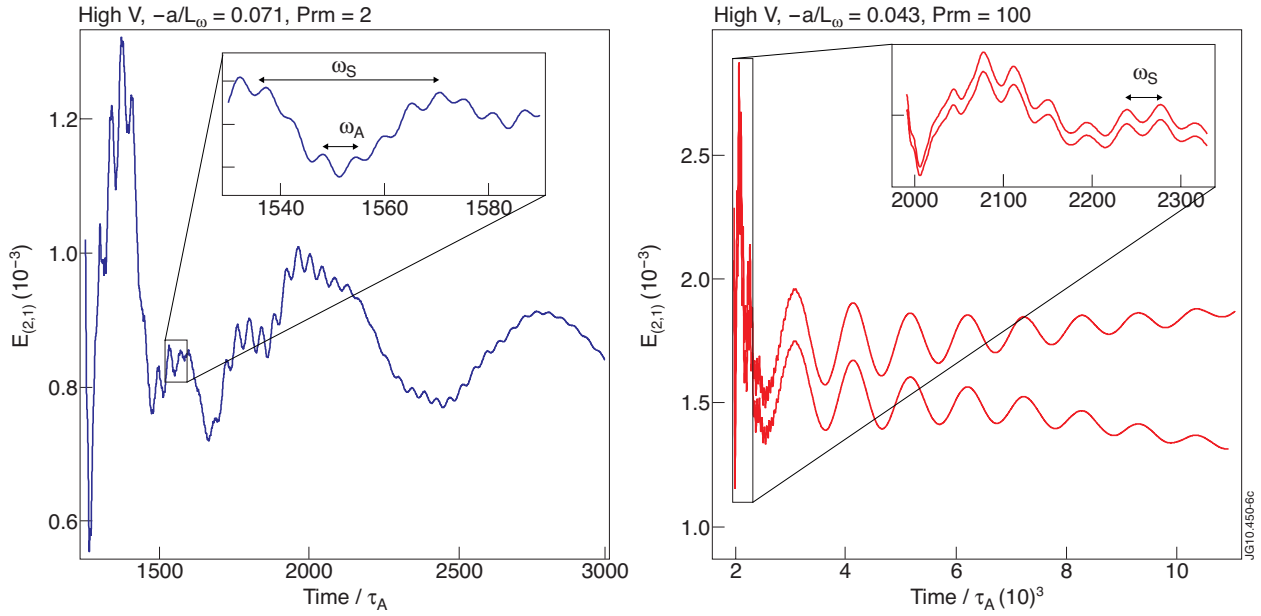

Figure 6: Oscillations of (2,1) magnetic energy after introduction of the seed island in "High V" simulations. At low viscosity and high velocity (left), characteristic pulsations are $\omega \sim \omega_s$ and $\omega \sim \omega_A$ (insert); oscillations at $\omega \sim \omega_s$ are rapidly damped (right, insert), and larger ones well below ω_s remain for a longer time.

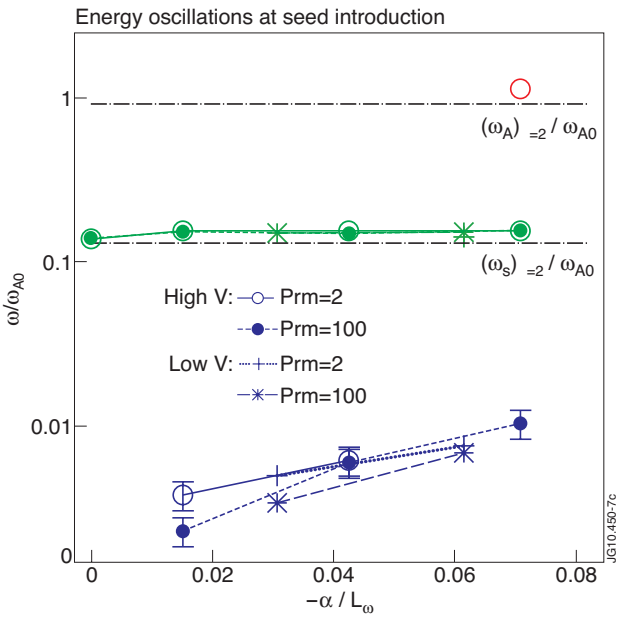

Figure 7: Characteristic pulsations of (2,1) magnetic energy as a function of flow shear parameter.

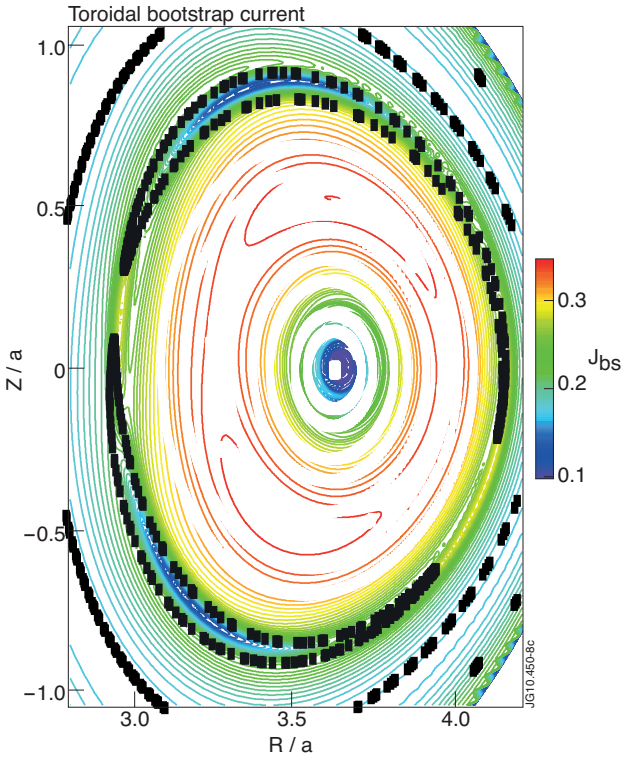

Figure 8: Contour of toroidal bootstrap current density for the High V case with $-a/L_\omega = 0.071$ and $W_{seed} = 0.053$, at $t/\tau_A = 5081$, together with a Poincaré plot showing the island separatrix.

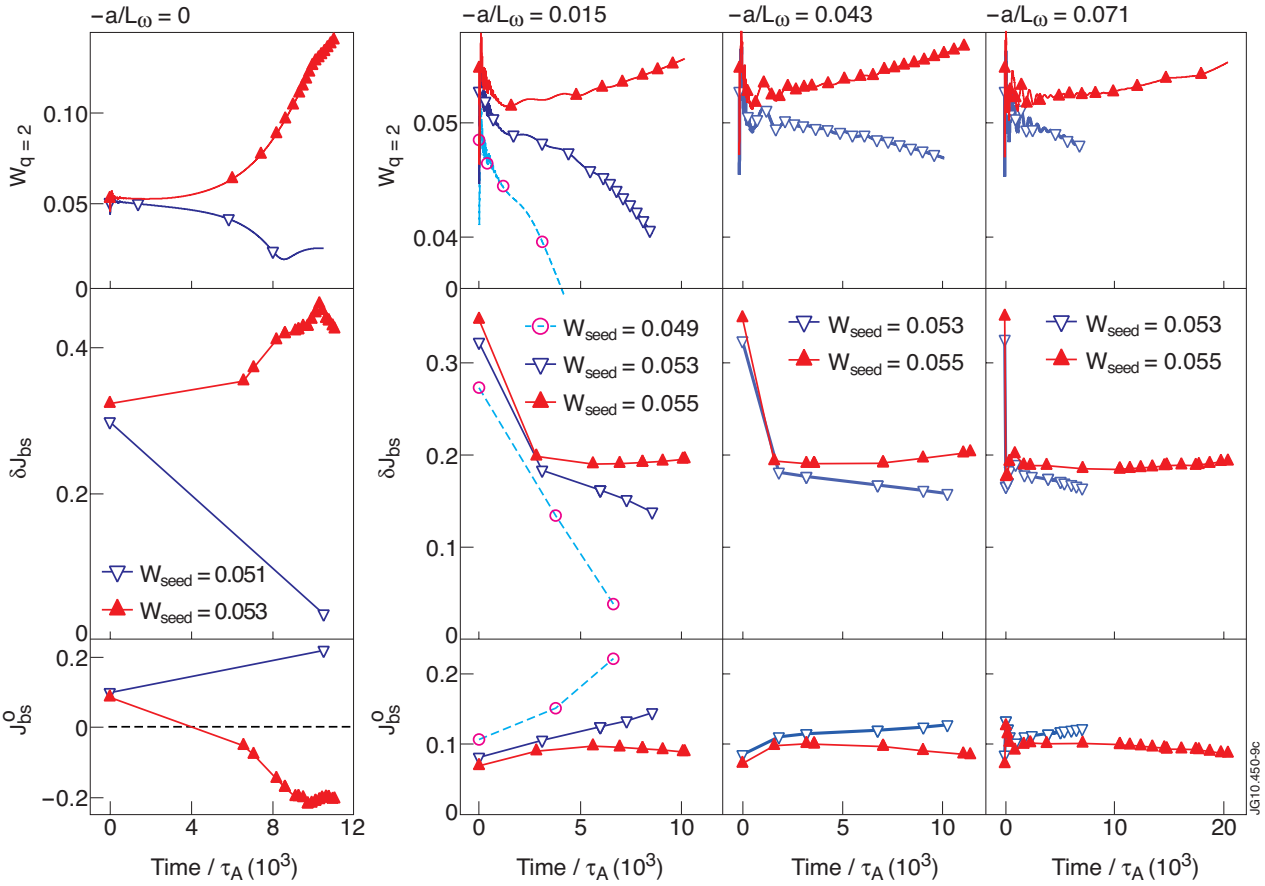

Figure 9: Island (top), bootstrap current perturbation (middle) and bootstrap current density at O-point (bottom) as a function of time for the different flow amplitudes in the "High V" case, and for Prm = 2.

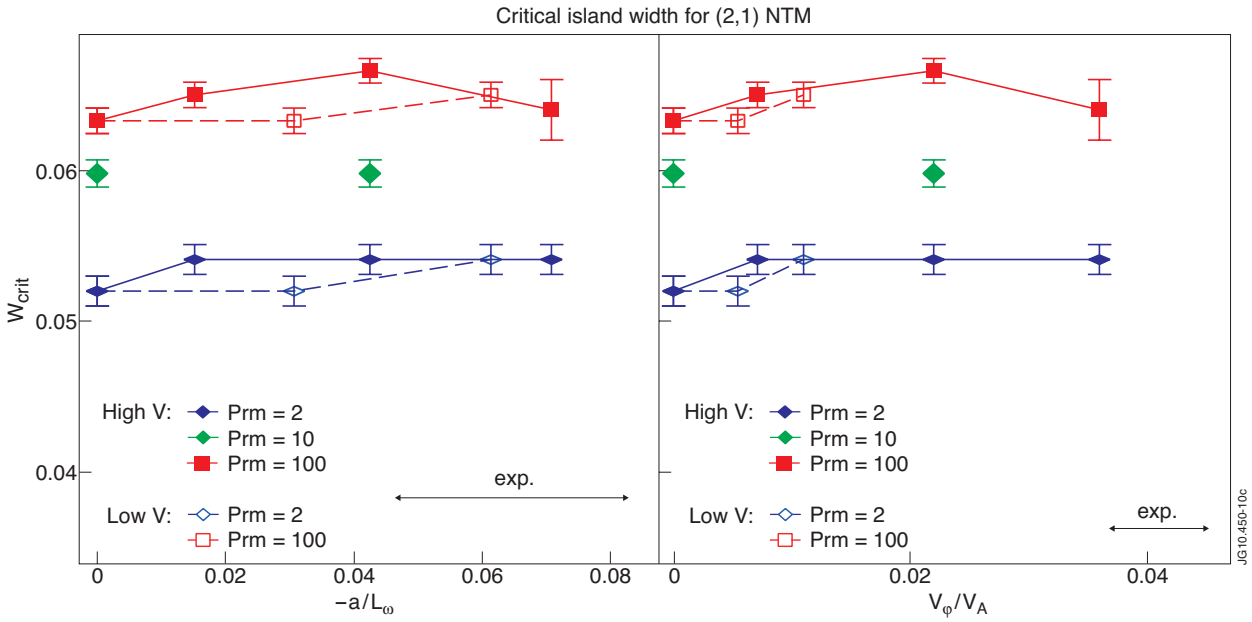

Figure 10: Critical island width as a function of the flow shear (left) and flow (right) at q = 2.

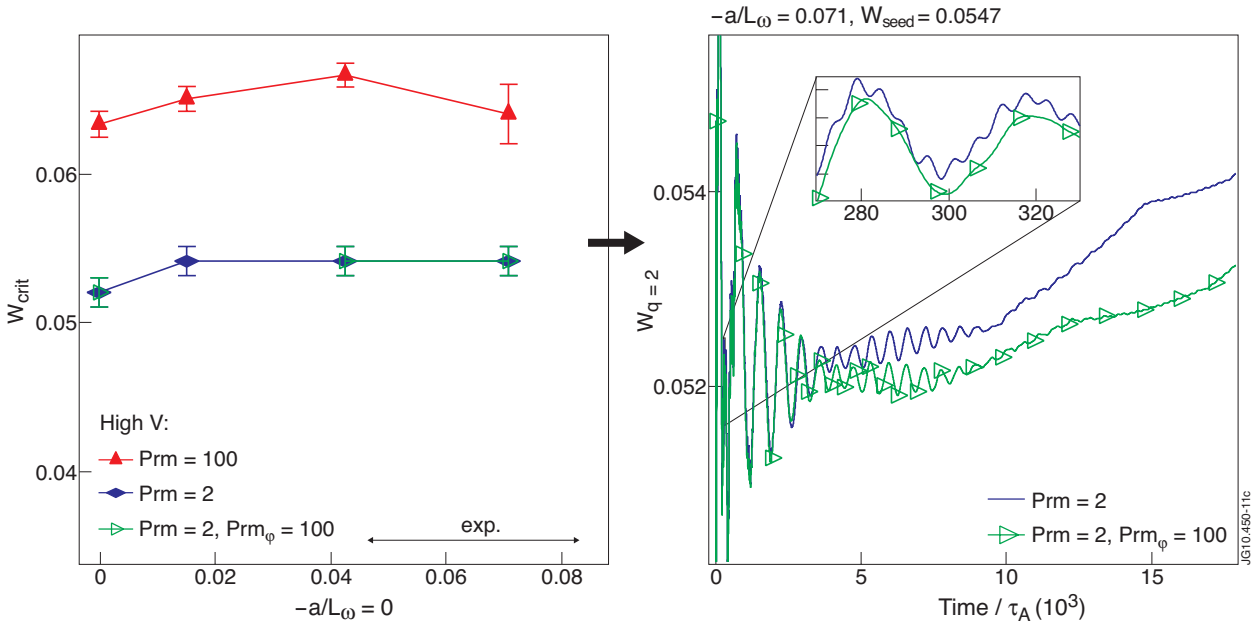

Figure 11: Critical island width as a function of rotation shear for isotropic and anisotropic viscosity (left); Island width dynamics in the high rotation shear case (right).

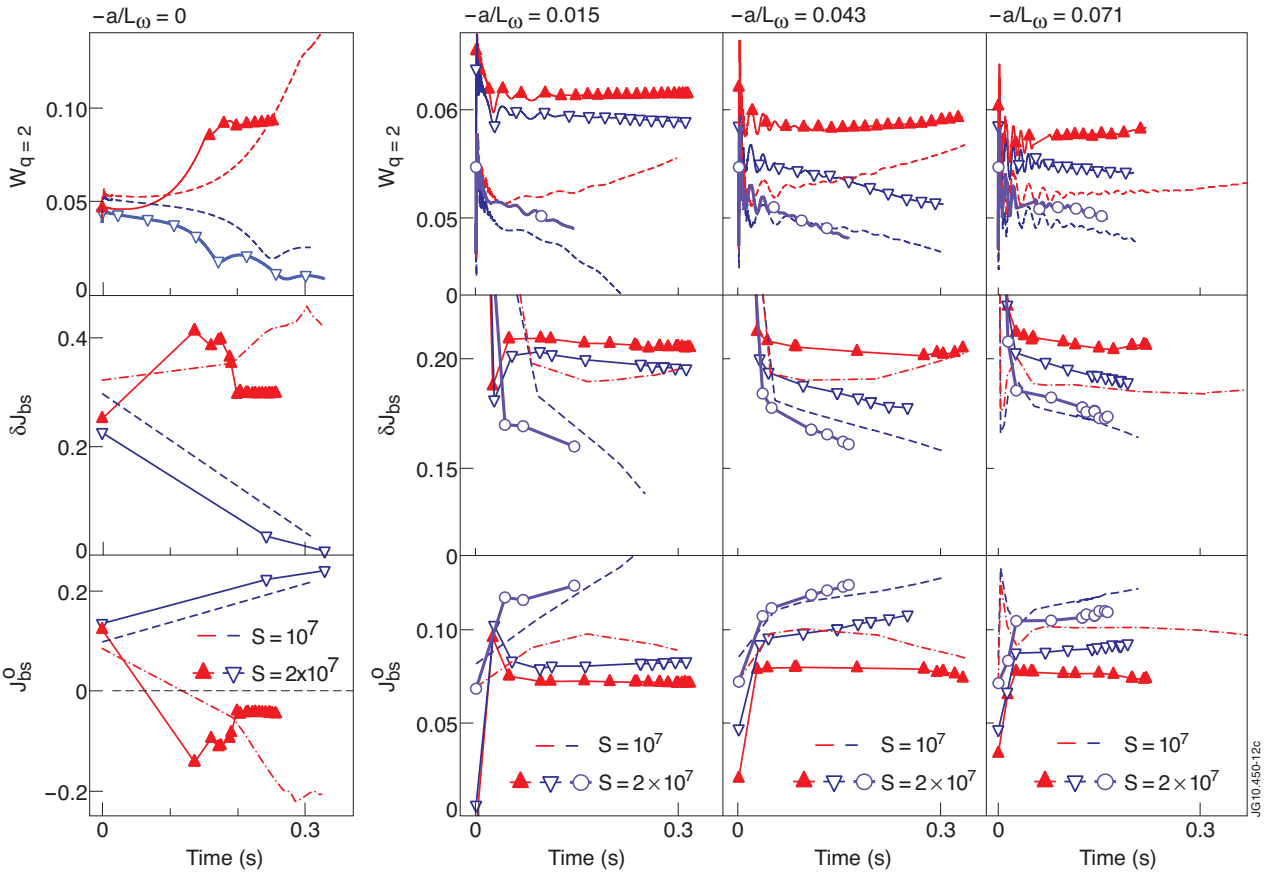

Figure 12. At Prm = 2: Island width (top), bootstrap current perturbation (middle) and bootstrap current density at O-point (bottom) as a function of the equivalent experimental time at $S = 2\times10^7$ (full lines) and $S = 10^7$ (dotted lines) for the different flow amplitudes in the "High V" case. Symbols ▲ and ▽ represents respectively the unstable and stable seeds; the symbol represent the dynamics at $S = 2 \times 10^7$ of the lowest unstable seed at $S = 10^7$.

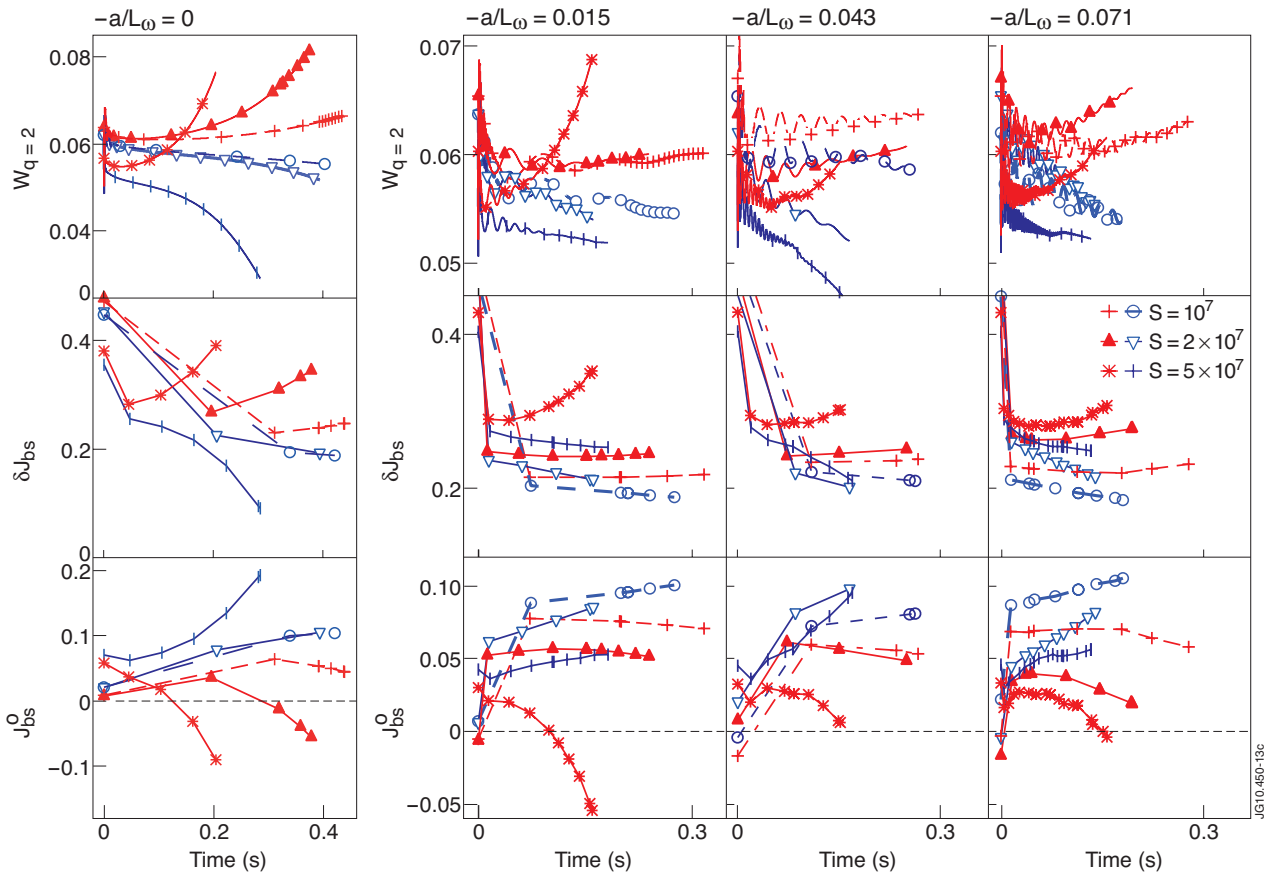

Figure 13: At Prm=100: Island width (top), bootstrap current perturbation (middle) and bootstrap current density at O-point (bottom) as a function of the equivalent experimental time at various S for the different flow amplitudes in the "High V" case. Symbols ▲ and ▽ represents respectively the unstable and stable seeds at $S = 10^7$, $S = 2 \times 10^7$ and $S = 5 \times 10^7$.

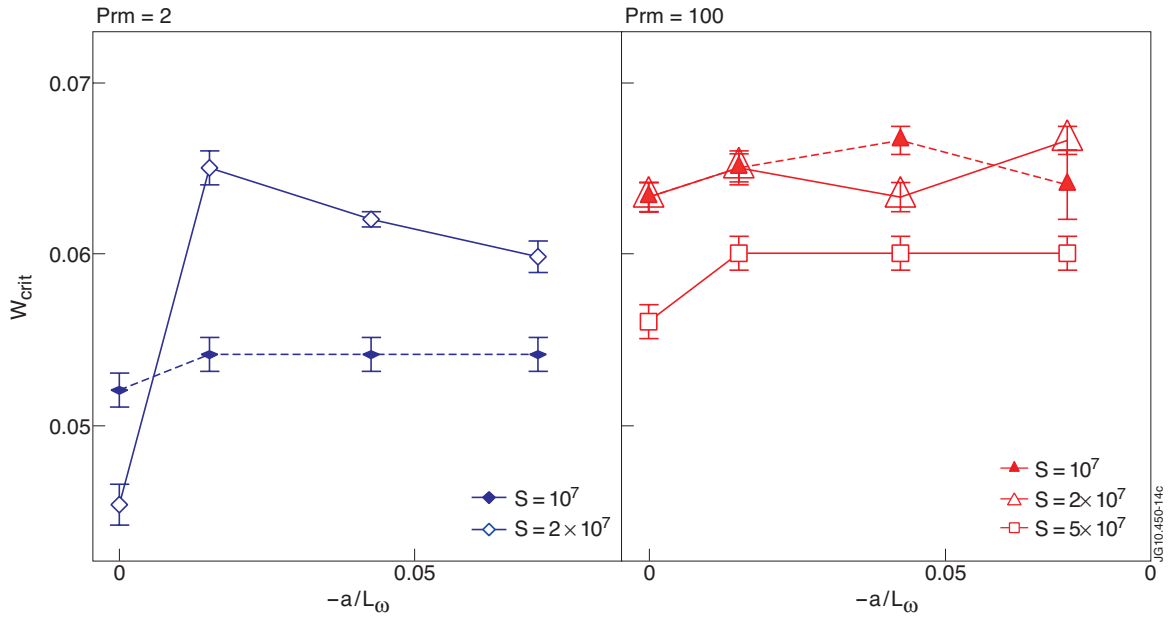

Figure 14. Critical island width as a function of rotation shear at Prm = 2 and Prm = 100 ("High V" case) for several Lundquist numbers.

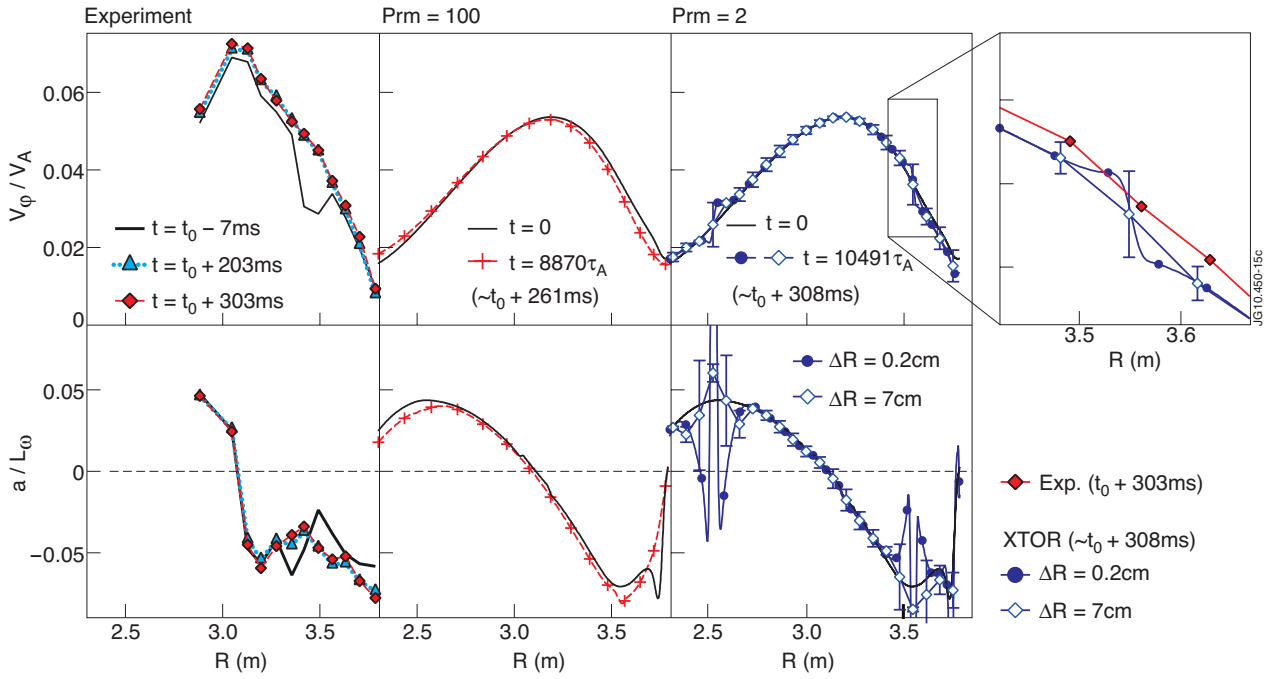

Figure 15. Impact of the (2,1) NTM on the n = 0 component of the toroidal flow (top) and toroidal flow shear (bottom) in the experiment (left), and in the simulations ("HighV" rotation profiles, right) at Prm = 100 (middle) and Prm = 2 (right). For Prm = 2, the flow shear has been calculated with the XTOR resolution (ΔR ~ 0.2cm), and with a resolution corresponding to that of the Charge Exchange diagnostic (ΔR ~ 7cm).